Contents

List of Figures

List of Tables

Hexapod-Based Active Stabilization System for Subsea Sensor Payloads

Saranya Mukherjee, AK Kundu

IRPE, University of Calcutta

1 Introduction

A Stewart platform, also known as a hexapod, is a type of parallel manipulator defined by a moving platform connected to a fixed base by six linear actuators (legs). This parallel structure grants the platform six degrees of freedom (6-DOF)—three translational and three rotational—while simultaneously providing high stiffness, exceptional load-carrying capacity, and precise kinematic control.

These characteristics make it ideal for tasks requiring high dynamic accuracy and rapid response, leading to uses in flight simulators, high-precision machining, and surgical systems. In the context of subsea robotics, the Stewart platform functions as an active stabilization end-effector for critical sensor payloads (like cameras or sonars). Its 6-DOF capability allows it to actively and instantaneously compensate for the base vehicle's motion (pitch, roll, and surge) and the unevenness of the seabed. This compensation ensures that the sensor maintains a constant, precise standoff distance and orientation relative to the target, which is essential for maximizing data quality during bathymetric surveys and targeted visual inspection. Furthermore, it allows for fine manipulation and micro-adjustments over specific seabed features, effectively decoupling the sensor's motion from the movement of the larger autonomous or remotely operated vehicle.

2 Stewart Platform

A Stewart Platform, formally known as a parallel manipulator or hexapod, is a mechanical device that represents a significant departure from conventional serial-link robots. Unlike an articulated arm (serial robot) where one joint follows another, the Stewart platform consists of a moving platform connected to a fixed base via six independent and synchronized linear actuators (legs). The key characteristic is that all six legs work in parallel to control the motion of the platform. This parallel arrangement is what grants the platform its immense mechanical advantages; the load and forces are distributed across multiple supports, it achieves exceptionally high stiffness, better precision, and superior dynamic response compared to serial manipulators of similar size. This architecture inherently restricts the accumulation of positioning errors, leading to high repeatability.

The power of the Stewart platform lies in its ability to control all six degrees of freedom (6-DOF) simultaneously: three translational motions (surge, sway, and heave—movement along X, Y, and Z axes) and three rotational motions (roll, pitch, and yaw). Control is achieved by precisely varying the length of each of the six actuators. To move the platform in any single direction or rotation, a coordinated change in the length of multiple actuators is required. This

coordination is computationally intensive, requiring a sophisticated inverse kinematic model to translate the desired position and orientation of the top platform into the specific lengths for the six individual actuators.

The unique combination of high dynamic performance and stability makes Stewart platforms indispensable in critical applications. Their original development was for use in aircraft and driving simulators where they must accurately replicate vehicle motion and forces instantaneously across all six axes to provide a realistic experience. In industrial settings, they are employed as high-speed positioners for tasks like laser welding, medical imaging, and orthopedic surgery positioning, where sub-millimeter accuracy is crucial. For subsea robotics, the parallel structure is invaluable for active vibration isolation and stabilization. By continuously adjusting the six legs in real-time based on sensor feedback (like altimeters or gyroscopes), the platform can effectively nullify the movement of the larger vehicle chassis, ensuring that the sensor payload remains perfectly level and at a precise distance from the seabed regardless of wave action or vehicle turbulence. This ability to instantly compensate for external disturbances is the core reason for their utility in dynamic and hostile environments.

3 Literature Review

We can split the existing literature on Stewart platforms into two major categories:

- Kinematic Modeling and Trajectory Planning: These involve understanding the platform's geometry and motion. Studies have documented various configurations, such as the 6-6 [5] and 6-3 [8] designs, which are defined by the spacing and arrangement of the joints on the fixed and mobile platforms. On the practical side, research has detailed the analysis of the platform's design, kinematic modeling, and trajectory generation. This work includes the application of inverse kinematics to define specific movements, such as point-to-point transfers via cycloidal trajectories [13] and more complex motions simulating oceanic waves. Furthermore, the computational efficiency of direct kinematics is studied to enable real-time feedback and allow for advanced control loops, such as "tracking error" supervisors.

- Control Strategies and Algorithms:

  Sliding Mode Control (SMC): SMC and its derivatives are popular for their robustness. A new controller based on the adaptive sliding-mode technique and a "Super-Twist" [6] state observer was proposed to manage nonlinear systems and external perturbations, demonstrating system stability. Similarly, other research introduced a novel adaptive super-twisting based smooth integral sliding mode controller (ASTSISMC) [12], where the super-twisting control replaces the discontinuous part of the integral sliding mode, and its gains adapt to the amplitude of disturbances, significantly improving disturbance rejection. A more generalized SMC [14] was also proposed and experimentally validated to improve the performance and positioning accuracy of Stewart platforms in industrial domains.

  Model Predictive Control (MPC): For dynamic trajectory following, a Switchable Model Predictive [16] Control (SMPC) strategy has been developed, focusing on replicating motion feelings during pilot training in flight simulators. Additionally, Iterative Learning Control (ILC) [7] has been used to accurately replicate a desired vibration response for road test simulation systems, demonstrating its utility in product quality enhancement and development time reduction for vehicle manufacturers.

Active Disturbance Rejection Control (ADRC): To combat issues like tracking lag from overload [10] and the impact of nonlinear factors, an improved Active Disturbance Rejection Control (ADRC) strategy for hydraulic-driven platforms was proposed. This method utilizes a cascaded extended state observer (ESO) to enhance the system's anti-interference ability and provide faster response times than traditional control methods.

4 Major issues in Stewart platform implementation

While Stewart platforms offer significant advantages, several challenges must be addressed for effective implementation:

- Complexity of Kinematics: The inverse kinematics of Stewart platforms is inherently complex due to the parallel structure and the interdependence of the six actuators. This complexity can lead to computational challenges, especially for real-time applications where rapid response is required.

- Control System Design: Designing robust control systems that can handle the nonlinear dynamics and potential disturbances in real-world applications is challenging. Advanced control strategies, such as sliding mode control or model predictive control, are often necessary but can be difficult to implement effectively.

- Mechanical Design and Fabrication: The precision required in the mechanical design and fabrication of Stewart platforms can be demanding. Any inaccuracies in the construction can lead to performance issues, such as reduced stiffness or increased backlash.

- Cost and Maintenance: Stewart platforms can be expensive to build and maintain due to their complexity and the precision required in their components. This can limit their accessibility for certain applications.

The foundational work aims at addressing the mechanical and cost related challenges through innovative design, which shall later pave the way for advanced control strategies to be implemented effectively.

5 Stewart platform IK

5.1 Define coordinate systems

To solve the inverse kinematics problem, we define two coordinate systems:

- Fixed Base Coordinate System($\sum_B$): Origin at the center of the fixed base platform.

- Moving Platform Coordinate System($\sum_P$): Origin at the center of the moving platform.

Hence, the geometry of the Stewart platform can be defined by:

- B_i : Position vectors of the base attachment points in $\sum_B$.

- P_i : Position vectors of the platform attachment points in $\sum_P$

- T: Translational vector of the platform with respect to the base.

- R: Rotation matrix representing the orientation of the platform with respect to the base.
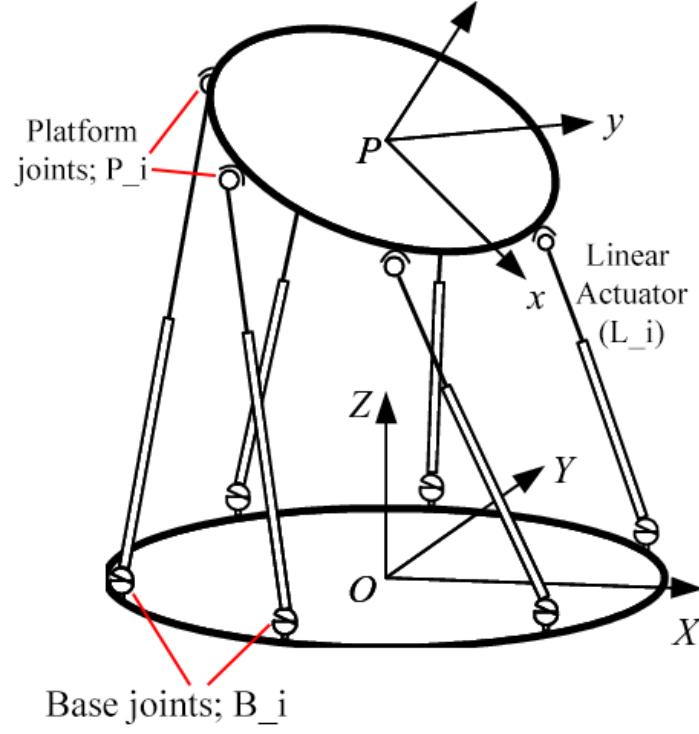
Figure 1: Schematic of a Stewart Platform showing the fixed base, moving platform, and six actuators.

5.2 Pose Representation

The pose of the moving platform is defined by a 6-element vector:

$$\mathbf{p} = \begin{bmatrix} x \\ y \\ z \\ \alpha \\ \beta \\ \gamma \end{bmatrix} \tag{1}$$

Where (x, y, z) is the translation and (α, β, γ) represent roll, pitch, and yaw in radians.

5.3 Rotation Matrix

Platform orientation is modeled by the combined rotation matrix:

$$\mathbf{R} = R_z(\gamma)R_y(\beta)R_x(\alpha) \tag{2}$$

Where:

$$R_x(\alpha) = \begin{bmatrix} 1 & 0 & 0 \\ 0 & \cos\alpha & -\sin\alpha \\ 0 & \sin\alpha & \cos\alpha \end{bmatrix} \quad R_y(\beta) = \begin{bmatrix} \cos\beta & 0 & \sin\beta \\ 0 & 1 & 0 \\ -\sin\beta & 0 & \cos\beta \end{bmatrix}$$

$$R_z(\gamma) = \begin{bmatrix} \cos\gamma & -\sin\gamma & 0 \\ \sin\gamma & \cos\gamma & 0 \\ 0 & 0 & 1 \end{bmatrix} \tag{3}$$

4

5.4 Inverse Kinematics

For each actuator: Given the base point $\mathbf{b}_i$ and platform point $\mathbf{p}_i$, The transformed platform joint position is:

$$\mathbf{P}_i^{world} = \mathbf{R} \cdot \mathbf{P}_i^{local} + \mathbf{T} \tag{4}$$

Where, $\mathbf{P}_i^{local}$ is the pose in terms of the 6-element vector, and $\mathbf{P}_i^{world}$ is its transformation.

So the vector along the actuator becomes:

$$\mathbf{L}_i = \mathbf{P}_i^{world} - \mathbf{B}_i \tag{5}$$

So the actual length of the actuator is:

$$L_i = ||\mathbf{L}_i|| = \sqrt{(P_{ix}^{world} - B_{ix})^2 + (P_{iy}^{world} - B_{iy})^2 + (P_{iz}^{world} - B_{iz})^2} \tag{6}$$

As is evident from the above equations, by substituting the desired pose parameters into the transformation equations, we can compute the required lengths of each of the six actuators to achieve that pose. But this process is computationally intensive due to the trigonometric functions involved in the rotation matrix. This specific issue can mostly be addressed by moderately sized lookup tables and interpolation techniques for real-time applications, aided by modern computational power and specifically designed hardware in embedded controllers.

6 Mechanical design of each actuator

Traditonal linear actuators used in Stewart platforms include hydraulic cylinders, electric linear actuators and alike but all of these options are expensive and complex to maintain in subsea environments. Not only this, but also either precision or speed is compromised in these traditional actuators. We have tried to come up with a novel mechanical design for each actuator that uses a combination of a common DC servos, and a scissor mechanism to convert rotary motion to linear motion while balancing not only both high precision and speed and cost-effectiveness, but also ease of maintenance in subsea environments and torque requirements within the limits of common hobby servos.

6.1 Basic framework

The basic framework of the proposed actuator design is shown in Fig. 2. The scissor mechanism consists of four arms of length L each, connected at a pivot point by two longer arms of length $2L$. The bottom ends of the shorter arms are connected to a fixed base, while the top ends are connected to the moving platform. The longer arms are connected to a servo motor at the pivot point, which drives the rotation of the mechanism. As the servo rotates, it changes the angle β between the longer arms and the horizontal plane. This rotation causes the scissor mechanism to extend or retract, changing the vertical height h of the moving platform. The relationship between the angle β and the height h can be derived using trigonometric principles, as discussed in the next section. The entire mechanism is based upon the assumption that the motion system stays symetrical about the vertical axis (marked in red). The mechanisms to enforce the later shall be discussed in the detailed design section.
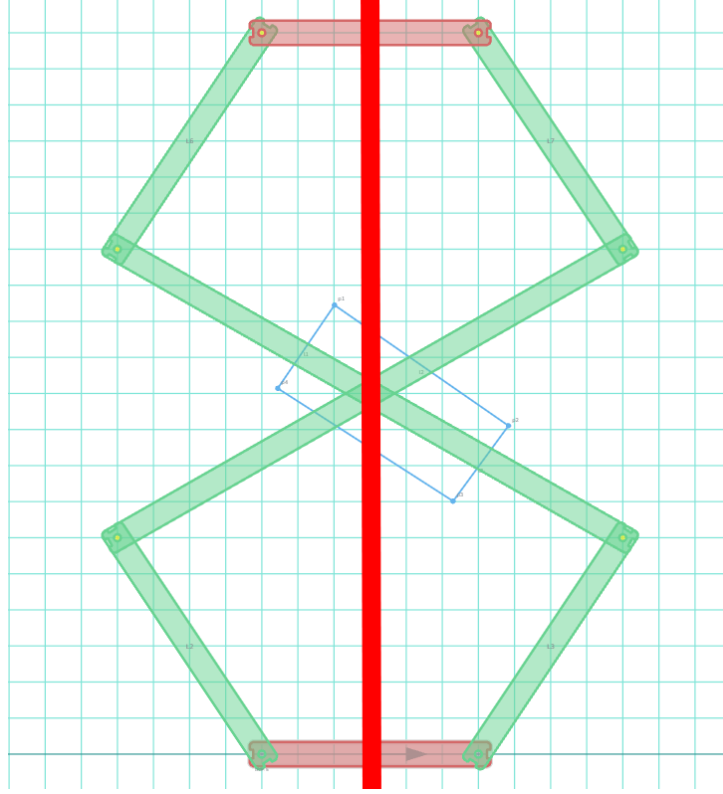
Figure 2: Schematic of the proposed actuator design using a scissor mechanism driven by a rotary servo motor.

6.2 IK equations

Fig. 3 shows the geometry of the scissor mechanism. From the figure, we shall focus on the triangle ABC. Here,

$$H = 2h$$

$$\beta = 2\alpha$$

$$\theta = \tan^{-1}\left(\frac{x}{h}\right)$$

$$\gamma = \frac{\pi}{2} - (\alpha + \theta)$$

$$d = \sqrt{x^2 + h^2}$$

Using the cosine rule in triangle ABC, we get:

$$\cos\gamma = \frac{L^2 + d^2 - L^2}{2Ld} = \frac{d}{2L}$$

Given that $\cos\gamma = \cos(\frac{\pi}{2} - \alpha - \theta) = \sin(\alpha + \theta)$, we have:

$$\alpha + \tan^{-1}\left(\frac{x}{h}\right) = \sin^{-1}\left(\frac{d}{2L}\right)$$

From this, we can solve for α:

$$\alpha = \sin^{-1}\left(\frac{\sqrt{x^2 + h^2}}{2L}\right) - \tan^{-1}\left(\frac{x}{h}\right)$$
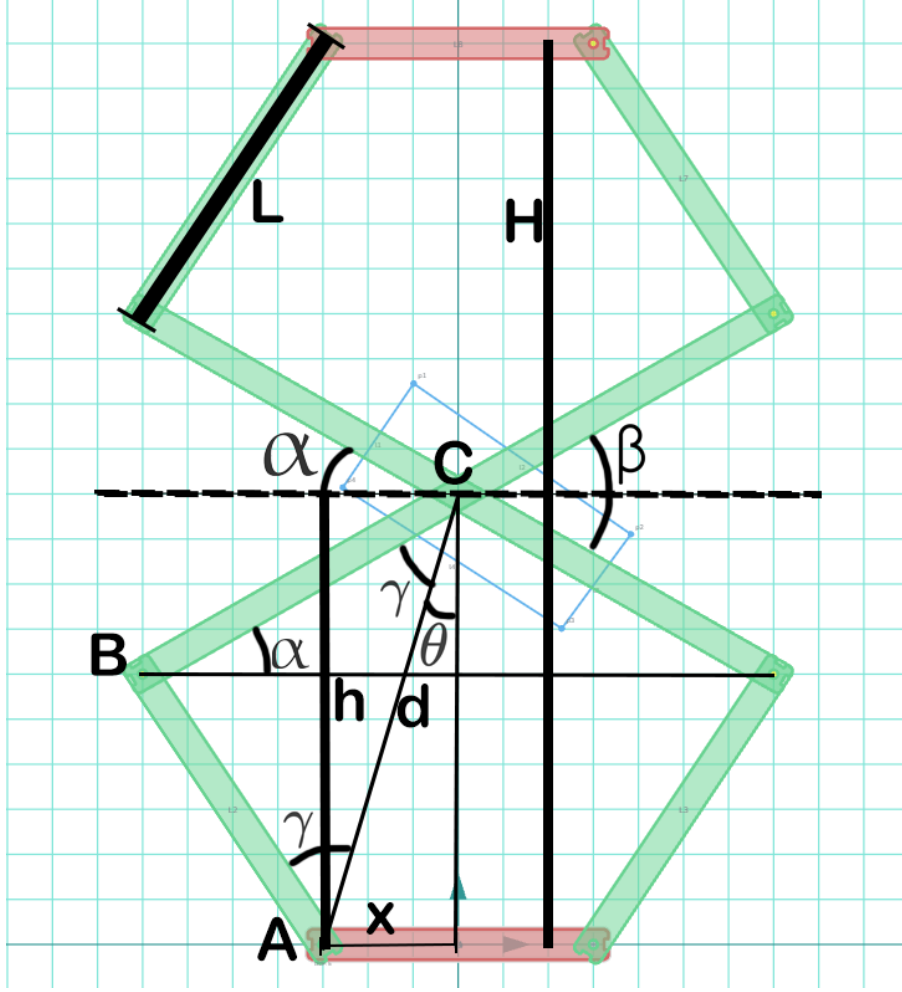
6

Figure 3: Geometry of the scissor mechanism showing each term.

Finally, we can compute β as:

$$\beta = 2 \left[\sin^{-1} \left(\frac{\sqrt{x^2 + \frac{H^2}{4}}}{2L} \right) - \tan^{-1} \left(\frac{2x}{H} \right) \right] \tag{7}$$

Since, all other parameters are in degrees,

$$\beta_{deg} = \beta \cdot \frac{180}{\pi} \tag{8}$$

Equation 7 gives us the inverse kinematics equation for the scissor mechanism, which shall serve as the basis for the control of each actuator in the Stewart platform.

IK equations are required to compute the required servo angle β for a desired actuator length H, but FK equations are also necessary inroder to formulate the control law and compute the dynamics of the motion of the systems. So the next section discusses the FK equations of the scissor mechanism.
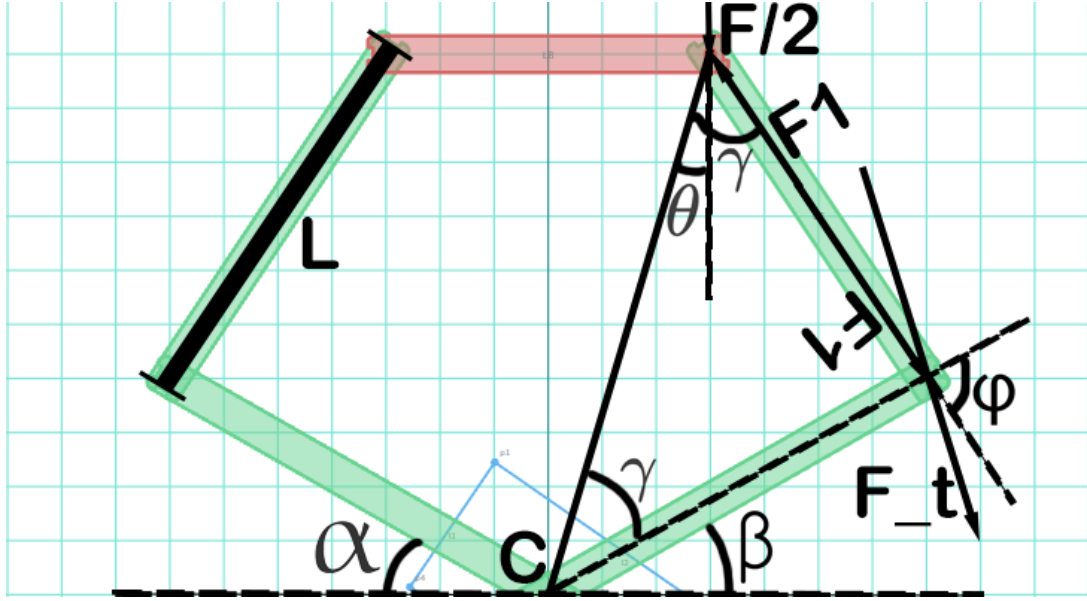
7

Figure 4: Free body diagram of the proposed mechanism.

6.3 FK equations

From Fig. 3, we can use the sine rule in triangle ABC to get:

$$h = L \sin \alpha + L \sqrt{1 - \frac{(L \cos \alpha - x)^2}{L^2}}$$

Hence, we can compute H as:

$$H = 2L \left[\sin \frac{\beta}{2} + \sqrt{1 - \frac{(L \cos \frac{\beta}{2} - x)^2}{L^2}} \right] \tag{9}$$

Now that we have both IK and FK equations for the scissor mechanism, we can proceed to the dynamic analysis for this mechanism.

6.4 Dynamical analysis

To derive the dynamics of the scissor mechanism, we can use differenciate the FK and IK equations with respect to time.

Differentiating Equation 9 with respect to time gives us the velocity relationship:

$$\frac{dH}{dt} = L \cdot \frac{d\beta}{dt} \left[\cos \frac{\beta}{2} + \frac{L}{\sqrt{1 - \frac{(L \cos \frac{\beta}{2} - x)^2}{L^2}}} \cdot \sin \frac{\beta}{2} \left(L \cos \frac{\beta}{2} - x \right) \right] \tag{10}$$
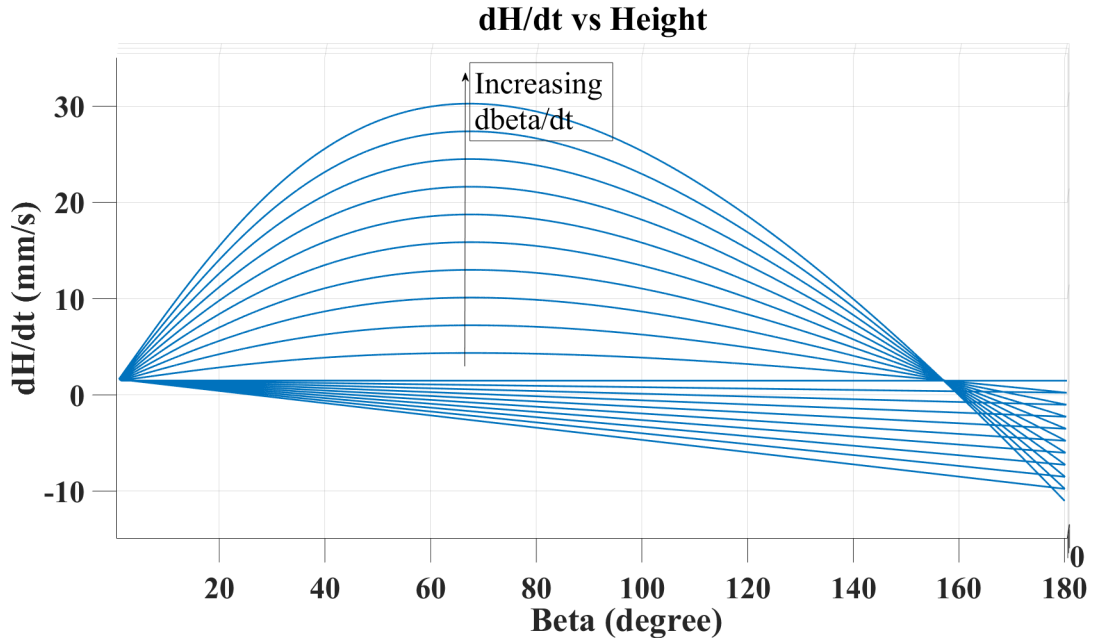
Similarly, differentiating Equation 7 with respect to time gives us:

$$\frac{d\beta}{dt} = \left(\frac{H}{16L} \cdot \frac{1}{\sqrt{1 - \frac{x^2 + \frac{H^2}{4}}{4L^2}} \cdot \sqrt{x^2 + \frac{H^2}{4}}} + \frac{x}{H^2} \cdot \frac{1}{1 + \frac{4x^2}{H^2}} \right) \frac{dH}{dt} \tag{11}$$
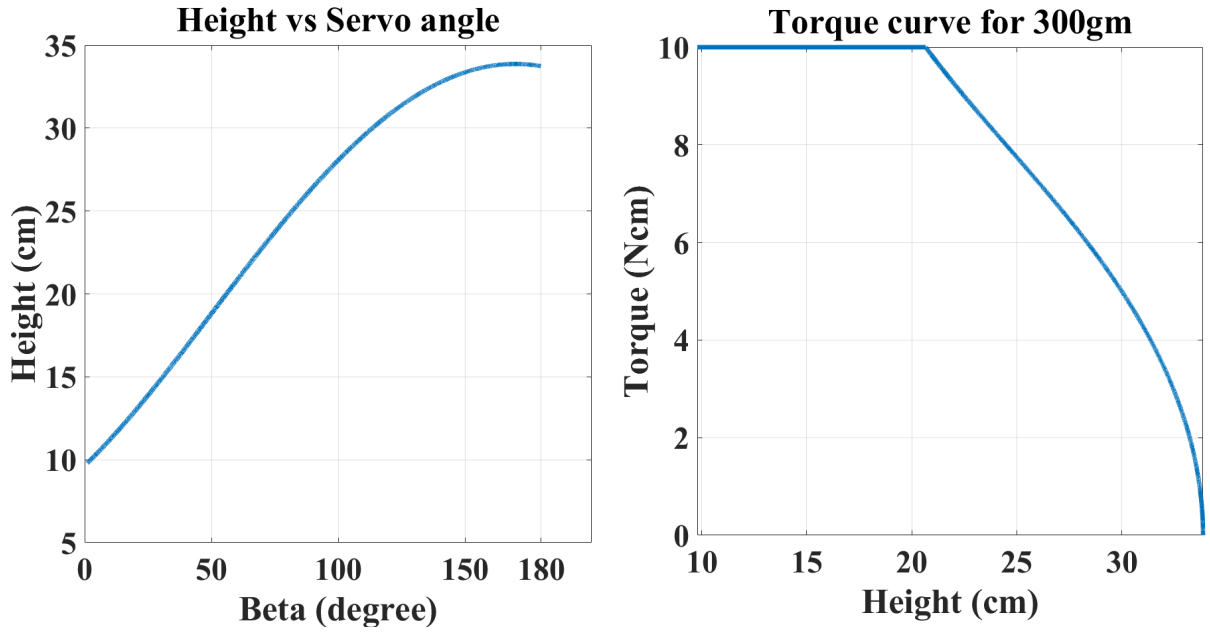
(a) Actuator length H vs β

(b) Torque on Servo τ vs H

(c) dH/dt vs β for varying $d\beta/dt$

Figure 5: System parameters for actuator with $L = 8.5cm, x = 1.5cm$

6.5 Static analysis

We need to compute the torque required at the servo motor to hold the platform at a certain height H. Fig. 4 shows the free body diagram of the scissor mechanism. Assuming that a force F acts at the center of the platform, since the mechanism is symmetrical about the vertical axis, each half will experience a force of $F/2$.

Balancing forces at the top platform link,

$$F_1 \cos(\gamma - \theta) = \frac{F}{2}$$

$$\phi = \pi - 2\gamma$$

9

Forces acting on the middle link will be F_1 on both sides for the link to be at equilibrium. So,

$$F_t = F_1 \sin \phi = F_1 \sin(\pi - 2\gamma) = F_1 \sin(2\gamma) = 2F_1 \sin \gamma \cos \gamma$$

$$F_t = \frac{F \sin \gamma \cos \gamma}{cos(\gamma - \theta)}$$

Now, given that the link has a length L and the torque is distributed evenly on both sides,

$$\tau = \frac{F \cdot L \sin (2 * (\theta + \alpha))}{\sin (2\theta + \alpha)} = \frac{2L \cdot F \sin(2\gamma)}{\sin \alpha} \tag{12}$$

Where, $\theta = \tan^{-1}\left(\frac{2x}{H}\right)$, $\gamma = \cos^{-1}\left(\frac{d}{2L}\right)$, and $d = \sqrt{x^2 + \frac{H^2}{4}}$.

6.6 Overall analysis

The following points summarize the performance analysis of the proposed actuator, drawing conclusions from the height, torque, and velocity curves(Fig. 5).

- Height-Angular Position Curve(Fig. 5a): The mechanism exhibits a large and highly linear region of operation, which is extremely desirable for simple and predictable control. The system provides a significant range of motion(ROM), extending from approximately $10cm$ to about $33.8cm$.

- Torque-Height Curve(Fig. 5b): Analyzing the torque requirements, the focus is placed on the region where the required torque falls below the typical $10N \cdot cm$ holding torque of standard commodity servos. Based on the curve for a $300gm$ force, the actuator provides an actually usable range of motion from approximately $21.3cm$ to $33.8cm$, which falls within the feasible operational zone of low-cost servos.

- Linear Velocity-Angular Velocity Curve(Fig. 5c): This study confirms the actuator's feasibility for operation in linear velocity mode in addition to linear position mode. The graph demonstrates that the mechanism can achieve a very high linear velocity for relatively low angular velocities of the servo motor. Notably, the highest point recorded shows a linear velocity of $30.6mm/s$ is achievable with an angular speed as low as $0.1rad/sec$ (approximately 5.7 degrees per second).

These results conclusively demonstrate that our proposed actuator not only provides a massive cost advantage over traditional linear actuators but also matches or surpasses them in every critical performance benchmark, including range of motion, control linearity, and attainable linear velocity.

7 Control system

Synergetic control theory (SCT) is a nonlinear control framework that shapes system behavior by forcing its states toward an invariant manifold, where the closed-loop dynamics [1] evolve smoothly and predictably. Unlike switching-based methods such as sliding-mode control [4], SCT [9] generates a continuous control law, eliminating chattering and yielding gentler actuator effort. Compared with classical linear approaches—like PID or state-feedback

Control Scheme	Reference	Key Contribution / Notes
Synergetic Control Theory (SCT)	[4, 9]	Demonstrates chattering-free dynamics vs. SMC and improved smoothness/robustness.
Sliding-Mode Control (SMC)	[6, 16]	Surveys robustness and finite-time convergence; discusses chattering issues.
Classical / Linear Controllers (PID, LQR, State Feedback)	[10, 12]	Evaluates classical PID limitations for nonlinear and uncertain systems.
Fuzzy Logic Controllers (FLC)	[3, 15]	Comprehensive survey of FLC and neuro-fuzzy control methods.
Neural-Network / Learning-Based Control	[2]	Overview of NN- and FLC-based control, stability issues, and design methods.
Adaptive / Backstepping / Modern Nonlinear Control	[2, 11]	Survey of adaptive, robust, and constrained backstepping methods.

Table 1: Representative References for Major Control Schemes

control—synergetic [11] control offers stronger robustness to parameter variations and non-linearities because its structure explicitly embeds system dynamics into a coordinated macro-variable [1].

Table 1 summarizes key references for various control schemes applied to Stewart platform like nonlinear systems. While PID controllers aim to regulate individual error signals independently, SCT coordinates multiple state variables toward a unified goal, improving performance in multi-state nonlinear systems. Relative to more computationally intensive intelligent controllers [2, 3, 15] (e.g., fuzzy logic or neural networks), SCT retains analytical transparency and simpler real-time implementation while still delivering high stability and fast convergence [1]. Overall, synergetic control theory provides a powerful middle ground: more robust and nonlinear-aware than classical controllers, smoother and easier to digitize than sliding-mode control, and more interpretable and lightweight than many AI-based schemes.

Moving forward, we plan to develop a synergetic control law for the Stewart platform using the derived inverse kinematics and dynamic model.

7.1 Define the macro-variable

To design a synergetic controller, we first define a macro-variable that captures the desired system behavior. Currently, we are looking for a effective position hold actuator that can reach the desired length without overshoot or oscillations. For the Stewart platform, we can define the macro-variable

$$\sigma = H_f - H \tag{13}$$

Where H_f is the desired actuator length and H is the current length.

7.2   Define the invariant manifold

Next, we define the invariant manifold that the system should converge to. A common choice is to set a first degree differencial equation for θ:

$$T \cdot \dot{\sigma} + \theta = 0 \tag{14}$$

Where, $\theta = f(\sigma)$ is a nonlinear function of σ that defines the desired dynamics on the manifold, and T is a designer chosen fixed parameter, that determines the convergence speed (smaller T means faster convergence). θ can be chosen as:

- invertible and differenciable

- $\theta(0) = 0$

- $\sigma \cdot \theta(\sigma) > 0$ for all $\sigma \neq 0$

We have chosen:

$$\theta = \sigma$$

7.3   Formulate the system dynamics

From eqn. 14,

$$T \cdot \left[\frac{dH_f}{dt} - \frac{dH}{dt} \right] + \left[H_f - H \right] = 0 \tag{15}$$
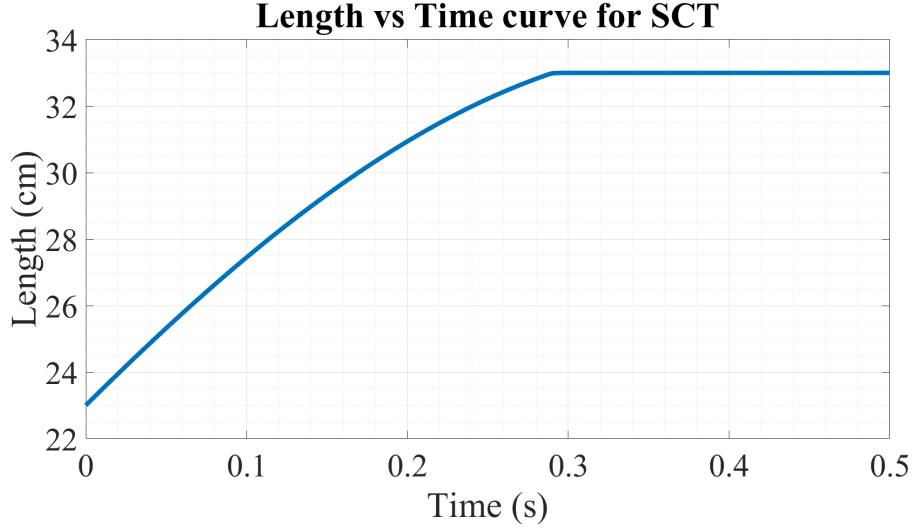
Since, H_f is constant for position hold,

$$T \cdot \left[-\frac{dH}{dt} \right] + \left[H_f - H \right] = 0$$
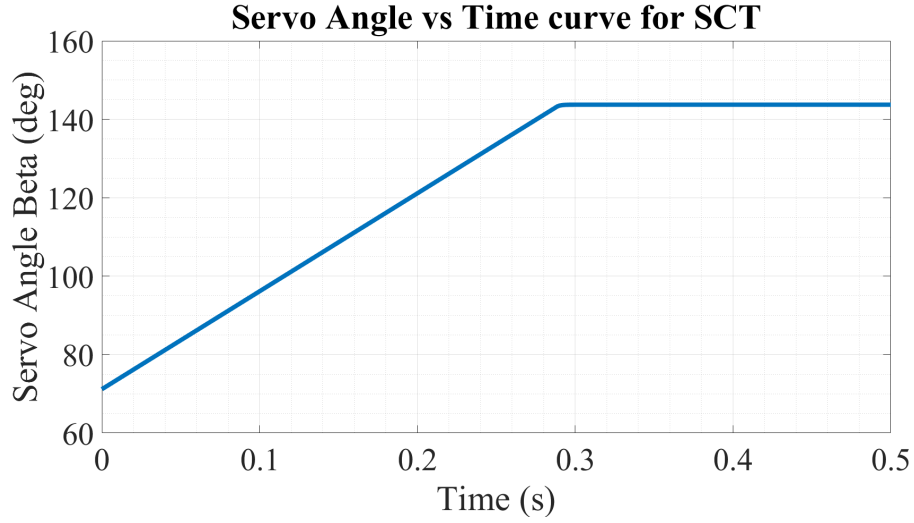
Now, substituting eqn. 9 and 10,

$$T \cdot \left[-L \cdot \frac{d\beta}{dt} \left[\cos \frac{\beta}{2} + \frac{L}{\sqrt{1 - \frac{(L \cos \frac{\beta}{2} - x)^2}{L^2}}} \cdot \sin \frac{\beta}{2} \left(L \cos \frac{\beta}{2} - x \right) \right] \right]$$
$$+ \left[H_f - 2L \left[\sin \frac{\beta}{2} + \sqrt{1 - \frac{(L \cos \frac{\beta}{2} - x)^2}{L^2}} \right] \right] = 0 \tag{16}$$

Now, solving for $\frac{d\beta}{dt}$,

$$\frac{d\beta}{dt} =$$

$$\frac{1}{T \cdot L \cdot \left[\cos \frac{\beta}{2} + \frac{L}{\sqrt{1 - \frac{(L \cos \frac{\beta}{2} - x)^2}{L^2}}} \cdot \sin \frac{\beta}{2} \left(L \cos \frac{\beta}{2} - x \right) \right]} \cdot \left[H_f - 2L \left[\sin \frac{\beta}{2} + \sqrt{1 - \frac{(L \cos \frac{\beta}{2} - x)^2}{L^2}} \right] \right]$$

$$\tag{17}$$

(a) Actuator length H vs Time

(b) Servo Angle β vs Time

Figure 6: Full scale movement vs time for SCT dynamics

7.4 Formulate the control law

Finally, we use eqn. 17 to get the control law:

$$\beta = \int \frac{d\beta}{dt} dt \tag{18}$$

Now descretizing the equation for digital implementation, we get:

$$\beta[k + 1] = \beta[k] + \frac{d\beta}{dt} \cdot \Delta t \tag{19}$$

Where $\beta[k]$ is the servo angle at time step k, and Δt is the sampling time, and $\beta[k + 1]$ is the updated servo angle to be sent to the servo motor.

7.5 Results

Fig. 6 shows the simulation results of the synergetic control law for a full scale movement from $H = 21.3cm$ to $H = 33.8cm$. As seen from Fig. 6a, the actuator reaches the desired length

13

without any overshoot or oscillations, demonstrating the effectiveness of the control law. Fig. 6b shows the corresponding servo angle β over time, which smoothly transitions to the required angle to achieve the desired actuator length.

With optimization of the parameter $T = 0.0001$, determined by limiting the maximum angular velocity of the servo motor at $4.36 rad/s$ or $250°/s$, allowing for ample headroom for real-world implementation,

- Convergence time(2% band): 0.255s

- Rise time: 0.162s - 0.049s(90% - 10%) = 0.113s

- Steady state error: 0cm

- Overshoot: NA

8   Conclusion

The work presented demonstrates the feasibility of a novel, low-cost scissor-mechanism actuator as a viable substitute for traditional linear actuators within a Stewart platform. Through the development of complete inverse and forward kinematic models, followed by detailed static, dynamic, and performance analyses, the proposed design shows excellent linearity, a wide usable range of motion, and actuator torque requirements that fit comfortably within the capabilities of standard hobby-grade servos.

Simulation results further confirm that the mechanism can achieve high linear velocities and maintain precise positioning despite its mechanical simplicity. Building on this mechanical foundation, a synergetic control law was formulated using the system's derived dynamics. The controller successfully drives the actuator to its target position without overshoot, oscillation, or chattering, achieving fast convergence and zero steady-state error. Together, the actuator design and the SCT-based control approach form a strong basis for implementing a complete, actively stabilized Stewart platform suitable for subsea sensing applications. Future work will integrate the actuator modules into the full hexapod structure and extend the synergetic controller to coordinate all six degrees of freedom for real-time platform stabilization.

References

[1] Azadeh Ahifar, Abolfazl Ranjbar Noee, and Zahra Rahmani. Terminal synergetic design of a nonlinear robot manipulator in the presence of disturbances. *COMPEL-The international journal for computation and mathematics in electrical and electronic engineering*, 37(1):208–223, 2018.

[2] Mojtaba Hadi Barhaghtalab, Mohammadreza Askari Sepestanaki, Saleh Mobayen, Abolfazl Jalilvand, Afef Fekih, and Vahid Meigoli. Design of an adaptive fuzzy-neural inference system-based control approach for robotic manipulators. *Applied Soft Computing*, 149:110970, 2023.

[3] Zoulikha Bouhamatou and Foudil Abedssemed. Fuzzy synergetic control for dynamic car-like mobile robot. *Acta Mechanica et Automatica*, 16(1):48–57, 2022.

[4] Nourdine Bounasla, Kamel Eddine Hemsas, and Hacene Mellah. Synergetic and sliding mode controls of a pmsm: A comparative study. *Journal of Electrical and Electronic Engineering*, 3(1-1):22–26, 2015.

[5] Bhaskar Dasgupta and TS1739334 Mruthyunjaya. The stewart platform manipulator: a review. *Mechanism and machine theory*, 35(1):15–40, 2000.

[6] Sajjad Keshtkar, Alexander S Poznyak, E Hernandez, and Armando Oropeza. Adaptive sliding-mode controller based on the "super-twist" state observer for control of the stewart platform. *Automation and Remote Control*, 78(7):1218–1233, 2017.

[7] Byeongsik Ko, Jong-Wook Park, and Dong W Kim. A study on iterative learning control for vibration of stewart platform. *International Journal of Control, Automation and Systems*, 15(1):258–266, 2017.

[8] PhD Stud Alina-Elena LUPULESCU. Studies on stewart platform–a review.

[9] Ahmed F Mutlak and Amjad Jaleel Humaidi. A comparative study of synergetic and sliding mode controllers for pendulum systems. *Journal Européen des Systèmes Automatisés*, 56(5):871, 2023.

[10] Xingyu Qu, Zhenyang Li, Qilong Chen, Chengkun Peng, and Qinghe Wang. Research on improved active disturbance rejection control strategy for hydraulic-driven stewart stabilization platform. *Industrial Robot: the international journal of robotics research and application*, 51(6):881–889, 2024.

[11] Zhengru Ren. A survey of modularized backstepping control design approaches to nonlinear ode systems. *arXiv preprint arXiv:2305.02066*, 2023.

[12] MK Safeena, KS Jiji, et al. Control of stewart platform using adaptive smooth integral sliding mode algorithm. *ISA transactions*, 156:99–108, 2025.

[13] Diego Silva, Julio Garrido, and Enrique Riveiro. Stewart platform motion control automation with industrial resources to perform cycloidal and oceanic wave trajectories. *Machines*, 10(8):711, 2022.

[14] Javier Velasco, Isidro Calvo, Oscar Barambones, Pablo Venegas, and Cristian Napole. Experimental validation of a sliding mode control for a stewart platform used in aerospace inspection applications. *Mathematics*, 8(11):2051, 2020.

[15] Fatemeh Zahedi and Zahra Zahedi. A review of neuro-fuzzy systems based on intelligent control. *Journal of Electrical and Electronic Engineering*, 3(2-1):58–61, 2015.

[16] Jiangwei Zhao, Zhengjia Xu, Dongsu Wu, Yingrui Cao, and Jinpeng Xie. Six-dof stewart platform motion simulator control using switchable model predictive control. *arXiv preprint arXiv:2503.11300*, 2025.